


Surface plasmon resonance effect enhanced upconversion luminescence in Ag modified NaYF₄: Yb/Er for photovoltaic efficiency improvement under solar irradiation

Shaoqi Zhu^{a,b}, Guanhong Lu^a, Xiao Wang^a, Tingsen Liu^c, Yongtai He^{c,*}, Jing Sun^a, Xiaofeng Xie^{a,b,**} 

^a Shanghai Institute of Ceramics, Chinese Academy of Sciences, 585 Heshuo Road, Shanghai, China

^b University of Chinese Academy of Sciences, 19 Yuquan Road, Beijing, China

^c School of Physics and Electrical Energy Engineering, Chuxiong Normal University, Chuxiong, China

ARTICLE INFO

Keywords:

Upconversion
Rare-earth
Plasmonic
Photovoltaic cell

ABSTRACT

Highly efficient upconversion materials are currently a major interest in photovoltaic research and industry. However, the existing upconversion luminescent materials exhibit low luminescence intensity and weak infrared light conversion efficiency, which impede the advancement of this field. In this study, core-shell structures of NaYF₄: Yb/Er@TiO₂ with plasmonic silver nanoparticles (Ag NPs) uniformly dispersed on the surface were successfully prepared by an in-situ reduction reaction. The incorporation of Ag NPs into the NaYF₄: Yb/Er@TiO₂ core-shell structures was found to result in a significant increase in photovoltaic power generation efficiency, reaching 4.81 % under sunlight irradiation. In comparison to the efficiencies of NaYF₄: Yb/Er@TiO₂ without silver powder (1.37 times higher) and NaYF₄: Yb/Er (2.19 times higher), both values demonstrate a notable improvement. This result is markedly superior to other documented instances of enhanced photovoltaic characteristics through spectral conversion. A mechanistic analysis indicates that this is due to the presence of silver nanoparticles, which enhance the electromagnetic field surrounding the converted luminescent particles on the surface of NaYF₄: Yb/Er@TiO₂. This improves their absorption and utilization of sunlight. The SPR-enhanced photovoltaic efficiency mechanism in this work is rarely reported and has important research and practical value.

1. Introduction

With the continuous development of renewable energy, the photovoltaic (PV) industry has also made great progress and become a key force in energy transition [1,2]. Further improving the photoelectric conversion efficiency of PV cells has become a new challenge for the development of PV technology, and even 1 % increase in efficiency is beneficial to economics and wider application [3,4]. Restricted by the bandgap of PV cells, the spectral response of PV cells is in the range of 320–1100 nm, and the infrared (IR) light, which accounts for about 43 % of the solar spectrum, is underutilized [5,6]. How to convert low-energy photons into high-energy photons is the key to further improve the efficiency of photovoltaic cells.

Rare-earth doped upconversion luminescent materials could convert infrared light into visible and ultraviolet light, and when integrated into

photovoltaic devices are able to fully utilize the solar spectrum for energy conversion, and show promising applications in improving photovoltaic performance [7,8]. The performance of the technology application is highly dependent on generating bright upconversion luminescence (UCL) or high upconversion quantum yields (UCQYs) [9]. To improve the luminescence efficiency of upconversion materials, current research focuses on two aspects: one is to optimize the structure and components of the materials, and the other is to improve the process of energy transmission. Various strategies have been used to enhance the intensity and efficiency of UCL, mainly including core-shell structures [10,11], ion doping [12], surface plasmon resonance [13], dye sensitization. Rare earth doped UCL materials consist of an inorganic matrix and rare earth doped ions. The UCL mainly relies on the step-like energy levels of the rare earth ions. To enhance the efficiency of UCL, sensitizers and activators are usually doped simultaneously. The sensitizer has a

* Corresponding author.

** Corresponding author. Shanghai Institute of Ceramics, Chinese Academy of Sciences, 585 Heshuo Road, Shanghai, China.

E-mail address: xxfshcn@163.com (X. Xie).

<https://doi.org/10.1016/j.renene.2025.123062>

Received 26 January 2025; Received in revised form 7 March 2025; Accepted 6 April 2025

Available online 7 April 2025

0960-1481/© 2025 Elsevier Ltd. All rights are reserved, including those for text and data mining, AI training, and similar technologies.

large absorption cross section for infrared light, while the activator such as Er^{3+} ions could emit visible light by electron leaps that fully utilize the energy transferred by the sensitizer. The higher concentration of sensitizer will be favorable to absorb more infrared light for energy conversion. However, there exists a concentration quenching effect. Liu et al. have verified that the proper proportion of Yb^{3+} ions doping in $\text{NaErF}_4\text{:x\%Yb@NaYF}_4$ nanoparticles has a positive effect on the NIR-II emission [14]. At the same time, to avoid cross-relaxation, the concentration of the activator should be kept to no more than 2 % as far as possible [15]. Therefore, the sensitizer concentration needs to be optimized for more efficient energy conversion.

In addition, by epitaxially growing an inert shell layer on the surface of the UCL core particles, the luminescent ions can be spatially isolated from external quenching sites, thus reducing surface bursting and enhancing luminescence. The thickness of the shell layer is a factor to be considered in the material design process. Li et al. observed size-dependent energy transfer effect in core-shell-shell $\text{NaYF}_4\text{@NaYF}_4\text{:Yb/Tm@NaYF}_4$ with depleted surface quenching by precising control the thickness of the middle shell [9]. To further expand the absorption of infrared light and enhance the emission of visible light during the UCL process, the surface plasmon resonance (SPR) effect on noble metal nanoparticles (such as Au, Ag, and Pt) can be exploited. When the frequencies of incident and emitted light overlap with the absorption frequency of the plasmon, the resonance can generate an enhanced electromagnetic field around the upconverted nanoparticles, which can increase the absorption cross-section as well as reduce the energy loss caused by non-radiative relaxation by improving the energy transfer efficiency [16]. This SPR effect is widely applied in fields such as nano-optics [17], catalysis [18], biomedical imaging and therapy [19, 20]. Xu et al. found that plasmonic Au nanoparticles and upconversion could improve solar energy utilization by capturing UV, visible, and NIR photons in enhancing the photocatalytic activity [21]. Compared with precious metals such as Au and Pt, Ag plasmas exhibit significant advantages in infrared light utilization and UCL enhancement, mainly attributed to their strong SPR effect (improving the absorption and scattering of infrared light), notable local electric field enhancement (promoting the excitation and emission of upconversion luminescent materials), low optical loss (especially in the infrared region), and relatively low cost. Although their chemical stability is slightly inferior, it can be improved through surface treatment. The resonance effect of Ag nanoparticles is usually manifested as localized surface plasmon resonance (LSPR), and the resonance wavelength depends on the size, shape, material of the particles and the refractive index of the surrounding medium [22,23]. Yang et al. reported ZIF-67/Ag NPs/ $\text{NaYF}_4\text{:Yb,Er}$ photocatalysts with outstanding light-absorbing qualities enhanced by LSPR effect [24]. The previous works demonstrate that the LSPR effect play an important role in enhancing the light-absorbing for photocatalytic performance. However, it remains a significant challenge to leverage the LSPR effect on enhancing the efficiency of PV cell.

Herein, we report a simple and novel strategy to grow plasma silver nanoparticles (Ag NPs) on upconversion particles $\text{NaYF}_4\text{:Yb/Er}$ (NYF) @ TiO_2 (denoted as NYF@ TiO_2 -Ag) by in-situ reduction method. To achieve efficient UCL performance for the purpose of enhancing the efficiency of photovoltaic cells, we systematically investigated the effects of rare earth ion doping concentration, shell layer thickness, and the LSPR effect of Ag NPs on the UCL. Upconversion particles were fabricated as coatings on the surface of photovoltaic cells, and the effect on the efficiency of photovoltaic cells was tested. NYF@ TiO_2 with plasmonic Ag NPs showed excellent PV cell efficiency enhancement. This work presents a new strategy to enhance the efficiency of photovoltaic cells by in-situ growth of plasmonic Ag NPs on upconversion particles.

2. Experimental section

2.1. Materials

Sodium citrate dihydrate, Sodium fluoride, Urea, Ytterbium nitrate, Erbium nitrate hexahydrate, Titanium(4+) tetrapropan-2-olate, Isopropanol and Silver(I) nitrate volumetric solution (0.01 mol/L) were purchased from Shanghai Titan Scientific Co., Ltd. Yttrium nitrate hydrate and Diethylenetriamine was purchased from Sinopharm Chemical Reagent Co., Ltd. Ethanol absolute was taken from Shanghai Lingfeng Chemical Reagent Co., Ltd. Deionized water was obtained from a Milli-Q system (Tondino Scientific (Shanghai) Co., Ltd). All chemicals are analytical grade and were used as received without any further purification.

2.2. Synthesis of $\text{NaYF}_4\text{:x\%Yb/2\%Er}$

$\text{NaYF}_4\text{:x\%Yb/2\%Er}$ ($x = 10, 20, 30, 40$ mol%) were synthesized by an improved hydrothermal method [21]. 3.52 mmol of Yttrium nitrate hydrate, 0.4 mmol of Ytterbium nitrate, 0.08 mmol of Erbium nitrate hexahydrate, were added to 65 mL of aqueous solution including 0.735 g of sodium citrate tribasic dihydrate and fully stirred for 1 h. Then, 0.84 g of Sodium fluoride and 6 g of urea were added to the above solution and further magnetically stirred for 1 h. The mixture was transferred into a 100 mL Teflon autoclave, and kept at 180 °C for 12 h. After cooling to room temperature, the obtained product was washed with deionized water and ethanol absolute for three times, respectively. Then, the product was dried at 80 °C for 12 h to obtain to final product $\text{NaYF}_4\text{:10\%Yb/2\%Er}$. The same preparation method was followed to obtain the $\text{NaYF}_4\text{:x\%Yb/2\%Er}$ ($x = 20, 30, 40$ mol%).

2.3. Synthesis of NYF@ TiO_2 (y mL)

NYF@ TiO_2 were synthesized by a hydrothermal method. As-obtained 0.05 g of $\text{NaYF}_4\text{:Yb/Er}$ as precursor and 0.04 mL Diethylenetriamine were dispersed in the 42 mL of Isopropanol and fully stirred for 10 min. Then, y mL Titanium (4+) tetrapropan-2-olate ($y = 0.5, 1.0, 1.5, 2.0$ mL) was added to the above solution and further magnetically stirred for 1 h. The mixture was transferred into a 100 mL Teflon autoclave, and kept at 200 °C for 24 h. After cooling to room temperature, the obtained product was washed with ethanol absolute for three times and dried at 80 °C for 12 h. Finally, the obtained product was calcined at 350 °C for 2 h to obtain the NYF@ TiO_2 ($y = 0.5, 1.0, 1.5, 2.0$ mL).

2.4. Synthesis of NYF@ TiO_2 @Ag NPs

The in-situ synthesis of Ag NPs on NYF@ TiO_2 was achieved by adding 0.08g of NYF@ TiO_2 to 20 mL of AgNO_3 solution and irradiating it under xenon lamp for 20 min.

2.5. Preparation of upconversion luminescent coatings

The sample was dispersed in the ethanol and sonicated for 1 h to obtain a solution ($m_{\text{samples}}\text{:}m_{\text{ethanol}} = 1\text{:}100$). Then, the solution was coated with non-woven cloth on the photovoltaic (PV) cell cover glass to obtain the coating. The silicon cell was commercially available N-type TOPCON crystalline silicon solar cell (18×18 cm, $J_{\text{SC}} = 0.0216$ mA cm^{-2} , $V_{\text{OC}} = 1.3955$ V, $\text{FF} = 69.9564\%$, $\text{Eff} = 21.1879\%$). The PV cover glass coated with the sample was placed on the silicon cell to form a mini-modules.

2.6. Characterization

The crystal structures of the samples were investigated by X-ray diffractometer (XRD, D8 ADVANCE, Bruker, Germany). The surface morphology and structure of the samples was characterized by a high

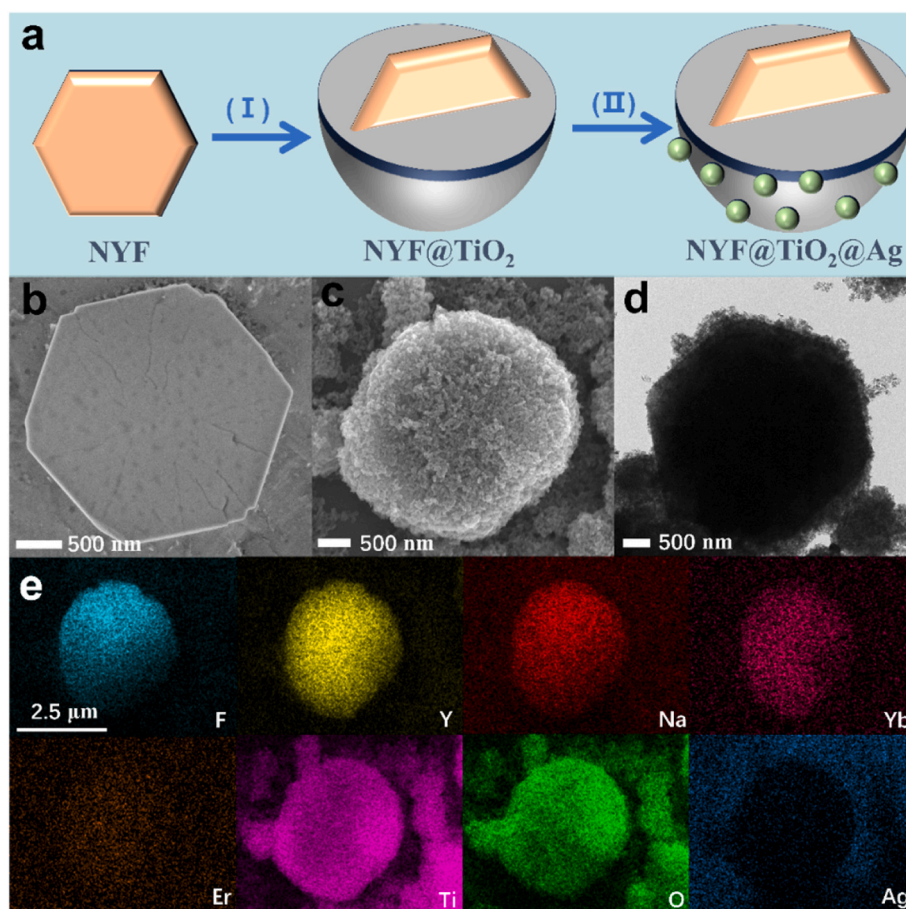


Fig. 1. (a) Schematic illustration for the synthesis of NYF@TiO₂@Ag via stepwise preparation, (b) SEM image of NaYF₄: 30 %Yb/2 %Er, (c) SEM image of NYF@TiO₂, (d) TEM image of NYF@TiO₂@Ag, (e) EDS images of NYF@TiO₂@Ag.

emission field resolution scanning electron microscope (SEM, Verios G4, FEI Corporation, America) and FEI Talos F200X G2 transmission electron microscopy (TEM). The element distribution of the core-shell structure was observed on a condenser aberration-corrected transmission electron microscope (EDS, Hitachi-HF5000, Japan). The optical absorption properties of the samples were measured by a UV-Vis-NIR spectrophotometer (PerkinElmer, model LAMBDA 1050). The up-conversion luminescence were measured under 980 nm excitation using a low temperature absorption spectrometer (FLS-980, Edinburgh, Britain). X-ray photoelectron spectroscopy (XPS) was implemented on a Thermo Scientific K-Alpha spectroscopy instrument. The I-V characteristics of PV mini-modules coated with the samples were measured by a solar simulator with 1 sun intensity (ProMoSim evo3, Strama-MPS, Germany).

3. Results and discussion

3.1. Morphology, structure, and characterization of NYF@TiO₂@Ag composites

The synthesis of NYF@TiO₂@Ag is divided into three main steps as shown in Fig. 1a. NYF micron hexagonal sheets are first fabricated using a hydrothermal method. The XRD diffraction peaks of NYF corresponds well to the JCPDS card No. 28-1192 with no impurity peaks (Fig. S1a). The morphological of the NYF micron hexagonal sheets are shown in Fig. 1b and Fig. S1. NYF hexagonal sheets have an average diameter of 3.5 μm and a thickness of about 140 nm (Figs. S1c and d). The EDS maps reveal that F, Na, Y, Yb, and Er elements are uniformly distributed in the NYF hexagonal sheets (Fig. S1e). The actual proportions of Yb and Er

elements in NaYF₄: 30 %Yb/2 %Er measured experimentally are close to the theoretical values, which are 32.69 % and 3.54 %, respectively (Table S1). Then the obtained NYF hexagonal sheets as core to construct TiO₂-coated core-shell structure by solvothermal method as shown in Fig. 1a. The synthesized TiO₂ is indexed to anatase (JCPDS card No. 21-1272) with a rod-like morphology of about 50 nm (Fig. S3), and the formation of the shell layer has no effect on the core crystal shape (Fig. S2).

And further, plasma Ag-loaded spherical NYF@TiO₂@Ag is prepared by in-situ reduction of AgNO₃ with shell TiO₂ under xenon lamp irradiation. As shown in the XRD pattern of Fig. S2, the obtained Ag is indexed to the Silver-3C pattern (JCPDS card No. 04-0783). The emerging diffraction peaks at 19.60° and 27.87° may be from residual AgNO₃. The TEM and EDS further characterized the structure and elemental distribution of the NYF@TiO₂ sample after Ag loading (Fig. 1d and e). The atomic content of Ag nanoparticles in NYF@TiO₂@Ag is 0.9 % as measured by XPS (Table S2). XPS analysis is implemented to describe the chemical state and composition of elements in the NYF@TiO₂ sample before and after in-situ reduction of Ag on the surface. As shown in Fig. 2a and b, XPS peaks of Ti and O elements are deconvoluted to confirm the variations in Ti³⁺ (O_{vs}) species and hydroxyl groups before in-situ reduction of Ag nanoparticles. Two peaks at 463.34 (Ti 2p_{1/2}) and 457.86 eV (Ti 2p_{3/2}) can be assigned to Ti³⁺ states for TiO₂ (Fig. 2a) [25]. The peaks of O 1s at 529.25 eV, 529.84 eV and 531.22 eV are owing to lattice oxygen (Ti-O-Ti), O-atoms near the O_{vs} and surface-absorbed oxygen species (-OH) of TiO₂, respectively (Fig. 2b) [26]. The content of O_{vs} in TiO₂ is calculated about 11.49 %. XPS survey spectrum imply the corresponding elements in NYF@TiO₂@Ag, with the peaks attributed to Na 1s, F 1s, O 1s, Ti 2p, Ag 3d, C 1s, Yb 4d, Er 4d and

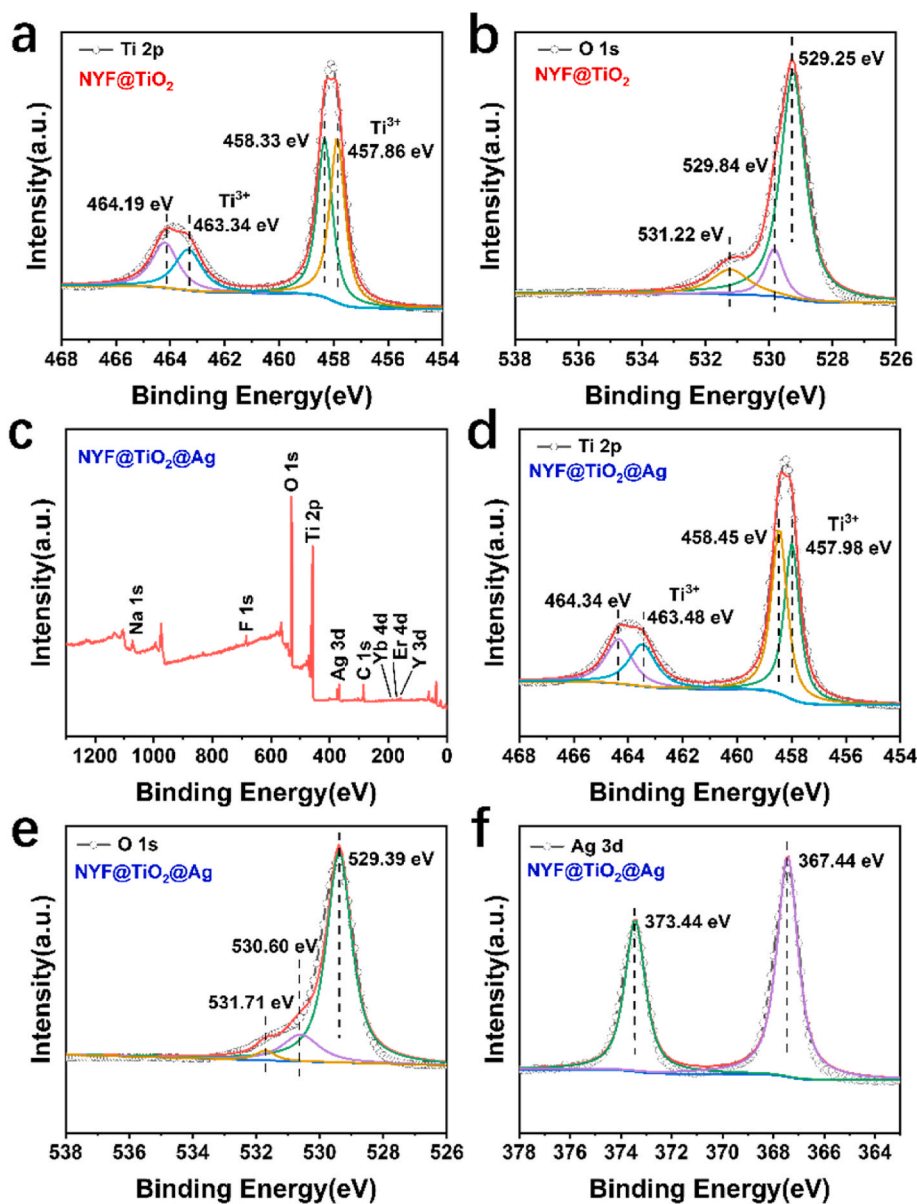


Fig. 2. XPS spectra of NYF@TiO₂ (a) in the Ti 2p and (b) O 1s regions, and NYF@TiO₂@Ag (c) survey spectrum, (d) in the Ti 2p, (e) in the O 1s and (f) Ag 3d regions.

Y 3d (Fig. 2c). After the in-situ reduction of AgNO₃ under xenon lamp irradiation, the peaks of Ti³⁺ and O-atoms near the O_{vs} shift toward higher binding energy (463.24 eV, 458.05 eV and 530.60 eV) (Fig. 2d and e). While the peaks at 367.44 eV and 373.44 eV in Fig. 3f correspond to 3d_{5/2} and 3d_{3/2} of Ag⁰, respectively [24]. It is deduced that the generation of slight Ag nanoparticles may be due to the transfer of electrons from Ti³⁺ on the surface of TiO₂ to Ag⁺, which causes Ag⁺ to undergo a reduction reaction to generate Ag particles, while Ti³⁺ itself undergoes an oxidation reaction to generate Ti⁴⁺. As shown in Fig. S4, the color of solution varies from white to dark gray after in-situ reduction of AgNO₃ by NYF@TiO₂, which implies the generation of Ag under electron transfer.

3.2. UCL performance and enhancement mechanism of NYF@TiO₂@Ag composites

The probability of energy transfer between Yb³⁺ and Er³⁺ is inversely proportional to the interionic distance between them. Therefore, higher molar concentrations of Yb³⁺ ions (ten times higher than the receptor) are typically used [27]. An optimized range of Yb³⁺ doping

concentrations was designed based on the previously reported Yb³⁺ to Er³⁺ concentration ratio of 18:2.

To reveal the effect of Yb³⁺ doping concentration on UCL, we prepare different concentrations of Yb³⁺ doped NaYF₄: x% Yb/Er (x = 10, 20, 30, 40). Fig. 3a shows UV-Vis-NIR absorption spectra for NaYF₄: x% Yb/Er (x = 10, 20, 30, 40). The absorption peak of NaYF₄: Yb/Er shows the intense light absorption in the 980 nm, which is caused by the ²F_{7/2} → ²F_{5/2} transition of Yb³⁺ [28]. And the intensity of the absorption peak enhances with the increase of Yb³⁺ ions doping concentration. As shown in Fig. 4b, the upconversion emission under 980 nm laser irradiation in the NaYF₄: Yb/Er with Yb³⁺ ions as the sensitizer and Er³⁺ ions as the activator are investigated. The spectral results show that the presence of increased Yb³⁺ content in the NaYF₄: Yb/Er samples contribute to an increase of the emission intensity. The sample with 30 mol% Yb³⁺ presents the optimum upconversion performance. The upconversion enhancement in the NaYF₄: Yb/Er should be ascribed to the nonlinear collaborative sensitization effect [32]. The enlarged Er³⁺-Er³⁺ ionic separation due to the increased concentration of Yb³⁺ can suppresses the cross-relaxation and enhances UCL accordingly [29,30]. The UCL intensity decreases instead when the Yb³⁺ ions concentration continued to

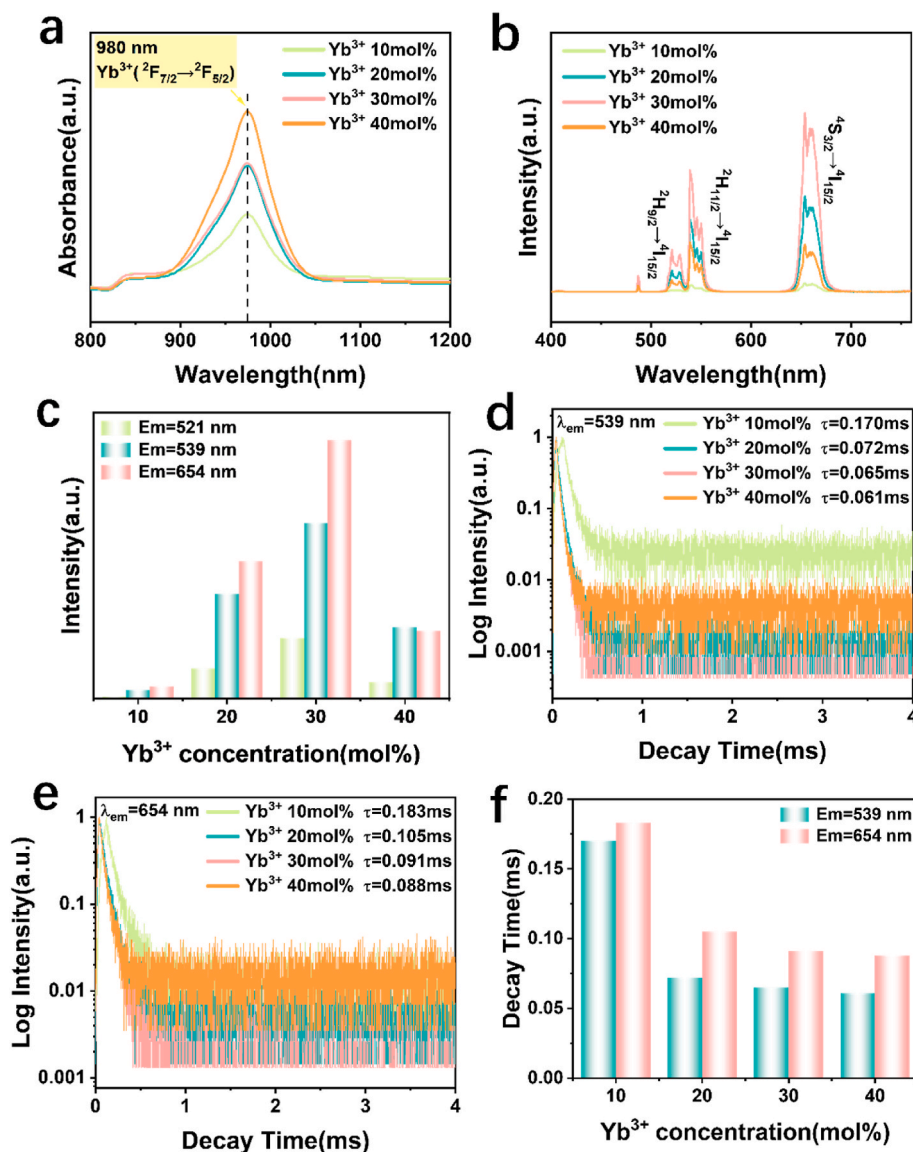


Fig. 3. (a) UV-Vis-NIR absorption spectra, (b) UCL spectra (excitation: 980 nm), (c) Comparison of UCL intensity at different Yb³⁺ doping concentrations, (d) Luminescence decay curves of NaYF₄: x% Yb/Er (x = 10, 20, 30, 40) at (d) 539 nm and (e) 654 nm, (f) Comparison of luminescence decay lifetimes at different Yb³⁺ doping concentrations.

increase (more than 30 mol%). This quenching of luminescence may be due to the reverse energy transfer from Er³⁺ to Yb³⁺, which resulting from the shortening of the distance between the sensitizers to activator ions [31]. This hypothesis is supported by the analysis of luminescence dynamics of the ²H_{11/2} and ⁴S_{3/2} energy level (Fig. 3d and e), in which the fluorescence decay lifetimes are reduced from 0.170 ms (Yb³⁺ 10 mol%) to 0.061 ms and 0.088 ms (Yb³⁺ 40 mol%), respectively [30]. Furthermore, the Yb³⁺ luminescence decay curves of NaYF₄: x% Yb/Er (x = 10, 20, 30, 40) are measured and the NaYF₄: x% Yb (x = 10, 20, 30, 40) without Er³⁺ doping is utilized as control samples (Fig. S5a, b). The energy transfer efficiency (η_{ET}) is quantified using equation (1) [9]:

$$\eta_{ET} = 1 - \frac{\tau_{Yb-Er}}{\tau_{Yb}} \quad (1)$$

where τ_{Yb-Er} and τ_{Yb} are the measured sensitizer Yb³⁺ ions luminescence decay lifetimes, with and without the activator Er³⁺ ions, respectively. Increasing the sensitizer Yb³⁺ ions doping concentration from 10 mol% to 40 mol% results in a decline in η_{ET} from 44.623 % to 2.027 %

(Fig. S5c), which again demonstrates the quenching effect on UCL caused by the shortened distance between the sensitizer Yb³⁺ ions and activator Er³⁺ ions. The NaYF₄: 30 %Yb/2 %Er reveals the most vigorous emission, thereby acting as a standard core matrix for subsequent TiO₂ shell encapsulation and upconversion enhancement investigation.

The core-shell engineering plays a significant role in protecting the UCL of NYF from quenching. To further optimize the UCL performance of the obtained NYF, the TiO₂-coated core-shell structure is designed and the thickness of the shell layer is optimized via adjusting the addition of titanium source, which is named NYF@TiO₂-y (y = 0.5, 1.0, 1.5, 2.0 mL). The thickness of the shell layer is mainly characterized by the degree of accumulation of TiO₂ nanoscale rod-like particles (Fig. 1c and Fig. S3). This is also shown in XRD pattern, where the intensity of the diffraction peaks of NYF decreases gradually with increasing thickness of TiO₂ (Fig. S6). The EDS shows the homogeneous distribution of each element in NYF@TiO₂ after TiO₂ shell coating (Fig. S7). TiO₂ nanoparticles can both absorb and reflect UV light and transmit visible light [32]. As shown in Fig. 4a, the UV-Vis-NIR absorption spectra shows the absorption peaks of TiO₂ in the UV region as well as the enhancement of light absorption across the wavelength band after TiO₂ coating. At low

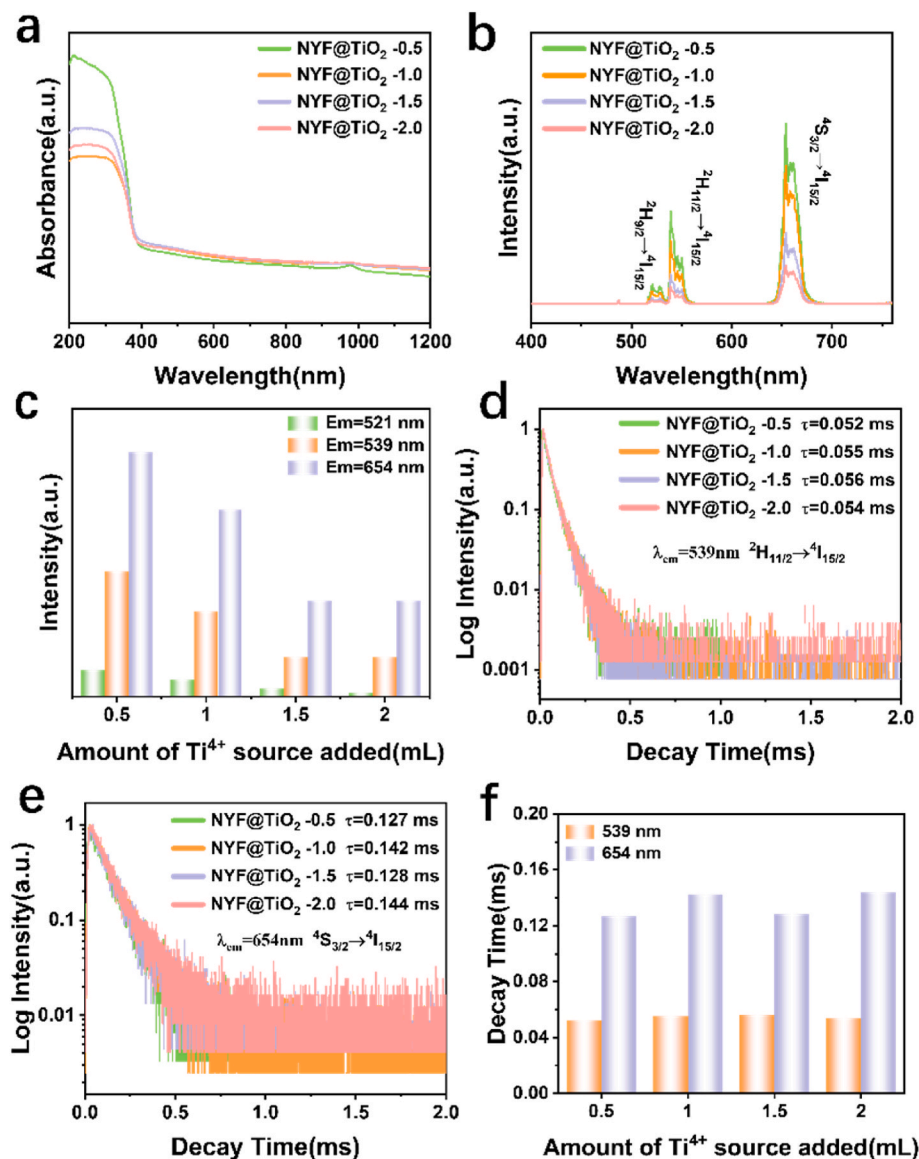


Fig. 4. (a) UV-Vis-NIR absorption spectra, (b) UCL spectra (excitation: 980 nm), (c) Comparison of UCL intensity at different shell thicknesses, (d) Luminescence decay curves of NYF@TiO₂-y (y = 0.5, 1.0, 1.5, 2.0) at (d) 539 nm and (e) 654 nm, (f) Comparison of luminescence decay lifetimes at different shell thicknesses.

concentrations, TiO₂ absorbs ultraviolet rays. However, at high concentrations, due to uneven dispersion and local enrichment, it affects the light transmittance, thus resulting in irregular changes in the ultraviolet region. The UCL spectra show that thinning the thickness of the shell layer in the NYF@TiO₂ core-shell structure enhances the luminescence intensity by 6.40, 3.14, 2.54 times at the emission peaks of 521 nm, 539 nm, and 654 nm, respectively (Fig. 4b and c). The corresponding SEM images are shown in Fig. S8, with the increase of titanium source addition during the synthesis process, the degree of Ti⁴⁺ hydrolysis increases, resulting in an increase in the generation of TiO₂ particles and a

Table 1

Electrical parameters of the photovoltaic cell covered with different samples under one standard solar intensity irradiation (AM1.5G, 100 mW/cm²).

Sample	J _{SC} (mA cm ⁻²)	V _{OC} (V)	FF (%)	Eff (%)	Overall increase (%)
Blank	0.0199	1.4026	70.8298	19.8251	–
NYF	0.0198	1.4262	71.7301	20.2609	+2.20
NYF@TiO ₂	0.0197	1.4435	72.1252	20.5197	+3.50
NYF@TiO ₂ @Ag	0.0197	1.4529	72.6494	20.7795	+4.81

thickening of the shell layer. The increase in the thickness of the shell layer reduces the absorption of 980 nm infrared light by Yb³⁺ ions, thus leading to a decrease in the intensity of UCL. To further investigate whether a thinner shell layer thickness will improve the UCL intensity, we reduce the amount of titanium source added in the control experiments to 0.1, 0.2, 0.3 and 0.4 mL, respectively. As shown in Fig. S9, when the titanium source is further reduced, it fails to form an effective shell layer encapsulation on the surface of the NYF, but instead introduces more surface defects, which can lead to a more severe luminescence quenching. However, the luminescence decay lifetimes of the NYF@TiO₂ remain almost unchanged during the adjusting of the shell layer thickness [33]. Therefore, independent regulation of luminescence intensity and luminescence decay lifetime is realized by constructing the form of NYF@TiO₂ core-shell structure [34]. We select NaYF₄: 30 % Yb/2 %Er@TiO₂-0.5 with optimal upconversion luminescence intensity for further in-situ reduction of AgNO₃ and use it as a functional coating to explore the effect on the conversion efficiency of photovoltaic cells.

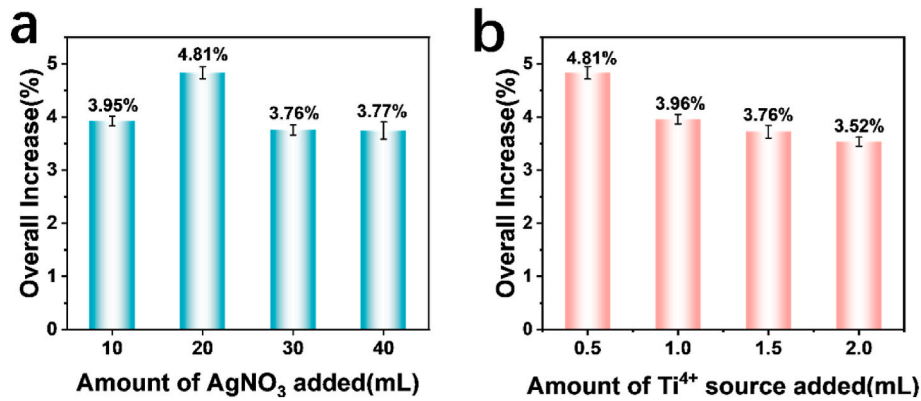


Fig. 5. Efficiency improvement of different coatings with as-prepared UCL samples on photovoltaic cell under solar irradiation: (a) variation in the amount of AgNO₃ added, (b) variation in the amount of Ti source added.

3.3. Effects of NYF@TiO₂@Ag UCL composites on PV cell efficiency

The influence of UCL and LSPR effect on the photovoltaic efficiency is explored. The as-obtained NYF, NYF@TiO₂ and NYF@TiO₂@Ag are homogeneously dispersed in ethanol, respectively. Uniform coatings are prepared on the surface of photovoltaic glass using nonwoven coating. As shown in Table 1, the effect of UCL materials on PV cells is tested separately with a solar simulator and the relative increase in efficiency is calculated. The initial efficiency of the PV cell is 21.879 %. After covering the photovoltaic glass, the efficiency of the photovoltaic cell is measured to be 19.8251 % as the transmittance decreased due to partial blocking of visible light. Further, the measured efficiencies of glass coated with different UCL materials covered with PV cells are 20.2609 % (NYF), 20.5197 % (NYF@TiO₂) and 20.7795 % (NYF@TiO₂@Ag), respectively. The calculated relative increases in PV cell efficiency are 2.20 % (NYF), 3.50 % (NYF@TiO₂) and 4.81 % (NYF@TiO₂@Ag), respectively. The results of the data show that the synergy between UCL and LSPR effect in the NYF@TiO₂@Ag contributes to the enhanced PV efficiency performance.

The NYF@TiO₂@Ag UCL material designed in this work can better utilize the infrared light in the solar spectrum for energy conversion and improve the power generation efficiency of photovoltaic cells. The N-type TOPCON photovoltaic cell used in this experiment represents the advanced level of the current photovoltaic industry, and its photoelectric efficiency is close to the theoretical limit. It is actually very difficult to further improve the efficiency on this basis, so the 4.81 % improvement in this study is a significant progress. At the same time, the fact that the PV cells used in the experiments are the latest industrial-grade products also makes the technology more valuable for practical application.

Furthermore, other comparative experiments of the samples for efficiency enhancement of PV cell are also exhibited in Table S3, Table S4, Table S5 and Fig. 5. The I-V curves of the PV cell covered with different samples under one standard solar intensity irradiation (AM1.5G, 100 mW/cm²) are shown in Fig. S11. First, we compare the reduction effect on AgNO₃ at different TiO₂ contents and accordingly tested the efficiency enhancement of PV cells as a coating. The results are shown in Table S3. The relative increase in PV cell efficiency is 3.96 ± 0.09 %, 3.76 ± 0.11 %, and 3.52 ± 0.08 % when the titanium source addition is 1.0, 1.5, and 2.0 mL, respectively. The enhancement effect of PV cell efficiency shows an increasing and then decreasing trend with the increase in the thickness of the TiO₂ shell layer. On the one hand, an increase in the thickness of the shell layer decreases the UCL efficiency, which is not conducive to improving the efficiency of PV cells. On the other hand, as the content of TiO₂ increases, there is a corresponding increase in Ti³⁺, which acts as an electron donor in the solution. It can transfer more electrons to Ag⁺ ions in AgNO₃ under xenon lamp irradiation, prompting the production of more Ag. Thus, the LSPR effect is

Table 2

List of relevant studies on upconversion or down-conversion materials enhancing the efficiency of solar cell.

Upconversion/down-conversion	PV cell efficiency enhancement	References
NaYF ₄ :Yb ³⁺ , Er ³⁺	2.06 %	[36]
NaYF ₄ :Eu ³⁺	3.46 %	[37]
YVO ₄ :Eu ³⁺ , Bi ³⁺	1.09 %	[38]
KY ₇ F ₂₂ :Yb ³⁺ , Er ³⁺	2.27 %	[39]
Zn _{0.4} Eu _{0.6} (TTA) ₂ PhenCl _{0.6}	2.57 %	[40]
NaYF ₄ :Yb ³⁺ /Er ³⁺ @TiO ₂ @Ag	4.81 %	This work

adjusting via oxygen vacancy engineering in NYF@TiO₂, which enhancing the abilities of NYF to absorb infrared light and emit visible light [35]. This improves the utilization of light in the PV cell, and ultimately leads to an increase in efficiency. Therefore, appropriate TiO₂ additions need to be controlled to maximize PV efficiency. We further investigate the effect of AgNO₃ content on Ag generation during the in-situ reduction process use NYF@TiO₂-0.5 in separate experiments and test the efficiency of the PV cells accordingly. As shown in Table S4, when the AgNO₃ content is 10, 40, and 60 mL, the PV cell efficiency increases relatively by 3.95 ± 0.09 %, 3.76 ± 0.09 %, and 3.77 ± 0.16 %, respectively. This is all lower than the increase in PV cell efficiency at a AgNO₃ content of 20 mL. This phenomenon also occurs similarly when varying the illumination time (Table S5). The optical photographs of the solution color of Ag synthesis reaction by in-situ reduction of AgNO₃ under different xenon lamp irradiation times are shown in Fig. S10. This shows a gradual darkening of the solution color as the xenon lamp irradiation time increases, indicating more Ag production. The reason why the lower PV cell efficiency in control subjects can be explained from the blank glass test data, as the PV cell efficiencies of the two blank glass coverings are 19.8251 % and 20.1191 %, thus leading to a deviation in the pattern of the relative increase in the PV cell efficiencies after coating coverage. While comparing the absolute value of increase in efficiency of PV cells, it has the highest value when the content of AgNO₃ is 20 mL and the illumination time is 20min. This indicates that there exists an optimal value for Ag generated, which is too little for full spectral conversion and too much for hindering the UCL process of NYF.

In addition, the PV cell enhancement performance of NYF@TiO₂@Ag material exceeds that of most NaYF₄-based and other host-based UCL or down-conversion materials (Table 2). Once again, we have demonstrated the superiority of our designed NYF@TiO₂@Ag materials for PV cell efficiency increase and the prospect of future applications.

3.4. SPR effect enhanced PV efficiency mechanisms

To shed light on the UCL and PV efficiency improvement mechanism,

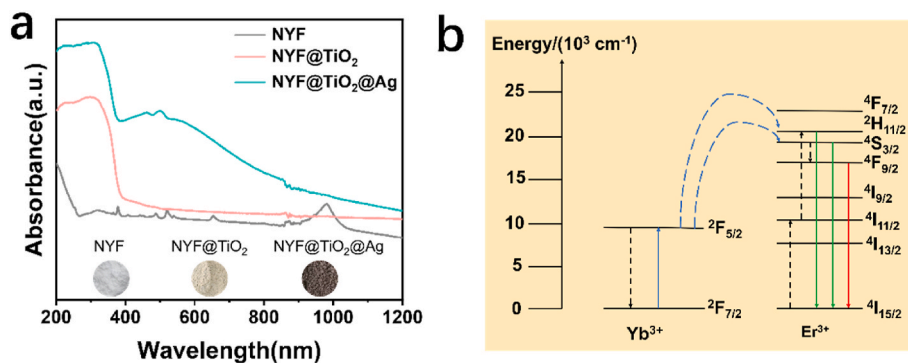


Fig. 6. (a) UV-Vis-NIR absorption spectra and photographs of powder samples of NYF, NYF@TiO₂ and NYF@TiO₂@Ag, (b) The upconversion process of NaYF₄:Yb/Er.

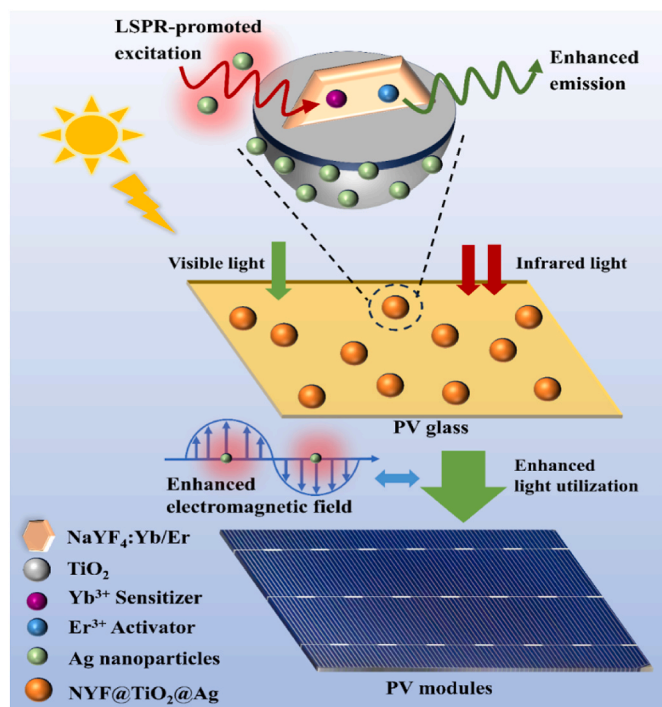


Fig. 7. Schematic diagram of NYF@TiO₂@Ag UCL material to improve the efficiency of PV cells.

the optical properties and band structures of as-prepared NYF@TiO₂@Ag samples are studied. As shown in Fig. 6a, the initial NYF exhibits characteristic absorption peak at 980 nm and the significant absorption peak in the UV region appear after the shell layer coating. The loading of Ag greatly enhances the ability of the obtained NYF@TiO₂@Ag samples to absorb light from the UV to the NIR region. The upconversion process diagram is drawn in Fig. 6b [41]. Yb³⁺ ions act as sensitizers, after absorbing 980 nm infrared light through the energy level jump from the ground state to the excited state ($2F_{7/2} \rightarrow 2F_{5/2}$ transition), and then transfer this part of the energy to the Er³⁺ ions (activator), in the form of radiation jump to emit visible light. Er³⁺ ions emit visible light at wavelengths of 520 nm, 539 nm, and 654 nm, which are originated from the $2H_{9/2} \rightarrow 4I_{15/2}$, $2H_{11/2} \rightarrow 4I_{15/2}$, $4S_{3/2} \rightarrow 4I_{15/2}$ electron transition, respectively [42,43]. Based on the above experimental and theoretical calculation results, a possible reaction mechanism of enhanced photovoltaic efficiency by upconversion luminescence is proposed and depicted in Fig. 7. Ag nanoparticles on the NYF@TiO₂ upconverted materials surface play an important role in the highly efficient spectral conversion by generating enhanced electromagnetic

fields through the localized surface plasmon resonance effect, which can increase the absorption of infrared light and amplify the emission of visible light. Thus, when NYF@TiO₂@Ag is applied to the surface of the PV cell as an upconversion functional coating, it increases the absorption of visible light by the PV cell and improves the photoelectric conversion efficiency.

4. Conclusion

In summary, we demonstrate that plasma-enhanced upconversion luminescent NaYF₄:Yb/Er@TiO₂@Ag material could be obtained by in-situ reduction AgNO₃ for efficient photovoltaic cell efficiency improvement. The concentration of Yb³⁺ and Er³⁺ ions in NaYF₄ are carefully tuned to achieve optimal upconversion luminescence performance. By adjusting the thickness of the TiO₂ shell layer, not only the upconversion luminescence is protected from quenching, but also the upconversion luminescence intensity and fluorescence lifetime are individually regulated. Further utilization of oxygen defects in TiO₂ for in-situ reduction of AgNO₃, and the sample exhibited the outstanding abilities for the solar spectral conversion and photovoltaic cell efficiency improvement. Our finding opens a new route to construct Ag nanoparticles on the NaYF₄:Yb/Er@TiO₂ upconverter surface through in-situ reduction, and provides a novel way to create higher efficient upconverter for converting solar energy into electricity. With the continuous development of materials science and nanotechnology, an increasing number of materials have shown potential for developing plasmonic resonance effects and have broad application prospects in the field of upconversion luminescence, such as transition metal sulfides, carbon-based materials, and chiral optical materials. Depending on the nature of the SPR material and its application characteristics, it can be expanded to more applications, such as bioimaging, optical storage, and information encryption.

CRediT authorship contribution statement

Shaoqi Zhu: Writing – original draft, Investigation, Conceptualization. **Guanhong Lu:** Methodology, Formal analysis, Data curation. **Xiao Wang:** Validation, Software, Resources. **Tingsen Liu:** Visualization, Validation, Resources. **Yongtai He:** Supervision, Resources, Funding acquisition. **Jing Sun:** Supervision, Resources, Project administration. **Xiaofeng Xie:** Writing – review & editing, Supervision, Funding acquisition.

Declaration of competing interest

The authors declare that they have no known competing financial interests or personal relationships that could have appeared to influence the work reported in this paper.

Acknowledgements

This study was financially supported by the Natural Science Foundation of Shanghai (22ZR1471800); Major Projects of Local Universities in Yunnan Province (No. 202101BA070001-039) and Hengdian Group Holding Co. LTD.

Appendix A. Supplementary data

Supplementary data to this article can be found online at <https://doi.org/10.1016/j.renene.2025.123062>.

References

- [1] Z. Zhou, J. Lv, C. Tan, L. Yang, Z. Wang, Emerging frontiers of 2D transition metal dichalcogenides in photovoltaics solar cell, *Adv. Funct. Mater.* 34 (2024) 2316175.
- [2] Q. Zhao, T. Liao, N.S. Awwad, Z. Hu, H. Zhang, Synergizing perovskite solar cell and thermally regenerative thermocapacitive cycle toward full-spectrum solar energy conversion, *Energy* 303 (2024) 132002.
- [3] C. Li, J. Chen, J. Chen, Y. Zhang, M. Li, H. Li, Boosting efficiency of CIGS solar cell by ferroelectric depolarization field, *Adv. Energy Mater.* 14 (2024) 2303162.
- [4] Z. Li, Y. Chen, R. Guo, S. Wang, W. Wang, T. Wang, S. Zhao, J. Li, J. Wu, Z. Jin, S. Wang, B. Wei, Doubling Power Conversion Efficiency of Si Solar Cells, *Adv. Mater.* 36 (2024) 2405724.
- [5] Y. Gao, D. Wu, Z. Dai, C. Wang, B. Chen, X. Zhang, A comprehensive review of the current status, developments, and outlooks of heat pipe photovoltaic and photovoltaic/thermal systems, *Renew. Energy* 207 (2023) 539–574.
- [6] S. Liu, C. Deng, M. Wang, A. Wei, T. Luo, H. Lu, X. Wen, M.-Y. Li, J. Zhang, Efficient quantum dot infrared photovoltaic with enhanced charge extraction via applying gradient electron transport layers, *Adv. Opt. Mater.* 12 (2024) 2303256.
- [7] B. Liu, Y. Wang, S. Bian, Z. Liu, Y. Wu, L. Shao, Y. Zhang, J. Lyu, L. Zhang, J. Mao, X. Bai, L. Xu, D. Zhou, B. Dong, H. Song, Perovskite solar cells with extremely high 24.6 efficiency through design of double electron transport layers and double luminescent converter layers, *Adv. Funct. Mater.* 34 (2024) 2401007.
- [8] W. Zhang, W. Zheng, P. Huang, D. Yang, Z. Shao, X. Chen, The marriage of perovskite nanocrystals with lanthanide-doped upconversion nanoparticles for advanced optoelectronic applications, *Aggregate* 5 (2024) e558.
- [9] F. Li, L. Tu, Y. Zhang, D. Huang, X. Liu, X. Zhang, J. Du, R. Fan, C. Yang, K. W. Krämer, J. Marques-Hueso, G. Chen, Size-dependent lanthanide energy transfer amplifies upconversion luminescence quantum yields, *Nat. Photonics* 18 (2024) 440–449.
- [10] Y. Xie, C. Cao, Y. Li, G. Ren, J. Wang, Upconversion enhancement in dye sensitized core/shell structure nanoparticles, *J. Lumin.* 258 (2023) 119786.
- [11] J. Huang, L. Yan, S. Liu, N. Song, Q. Zhang, B. Zhou, Dynamic control of orthogonal upconversion in migratory core-shell nanostructure toward information security, *Adv. Funct. Mater.* 31 (2021) 2009796.
- [12] J. Ma, Y. Wei, T. Liu, L. Xu, T. Wang, Z. Song, J. Qiu, Y. Li, Simultaneous enhancement upconversion luminescence and photocatalytic properties of BiOBr: Yb³⁺, Er³⁺ nanosheets by optically inert ions doping, *J. Lumin.* 260 (2023) 119860.
- [13] H. Xia, D. Li, J. Shang, Y. Ji, X. Yin, G. Fang, W. Xu, B. Dong, Electrically sensitive plasmonic photonic crystals for dynamic upconversion manipulation, *Adv. Funct. Mater.* 33 (2023) 2304045.
- [14] X. Liu, T. Liu, L. Tu, J. Zuo, J. Li, Y. Feng, C. Yao, Enhancing NIR-II upconversion monochromatic emission for temperature sensing, *Small* 20 (2024) 2308748.
- [15] W. Gao, Y. Xing, B. Chen, L. Shao, J. Zhang, X. Yan, Q. Han, C. Zhang, L. Liu, J. Dong, Enhancing red upconversion emission in NaErF₄@NaYF₄ core-shell nanoparticles by introducing Yb³⁺ ions as energy trapping centers, *J. Alloys Compd.* 936 (2023) 168371.
- [16] T. Liu, X. Liu, Y. Feng, C.-J. Yao, Advances in plasmonic enhanced luminescence of upconversion nanoparticles, *Mater. Today Chem.* 34 (2023) 101788.
- [17] A. Garg, E. Mejia, W. Nam, M. Nie, W. Wang, P. Vikesland, W. Zhou, Microporous multiresonant plasmonic meshes by hierarchical micro-nanoimprinting for bio-interfaced SERS imaging and nonlinear nano-optics, *Small* 18 (2022) 2106887.
- [18] Z. Li, J. Zi, X. Luan, Y. Zhong, M. Qu, Y. Wang, Z. Lian, Localized surface plasmon resonance promotes metal-organic framework-based photocatalytic hydrogen evolution, *Adv. Funct. Mater.* 33 (2023) 2303069.
- [19] J.-S. Lin, X.-D. Tian, G. Li, F.-L. Zhang, Y. Wang, J.-F. Li, Advanced plasmonic technologies for multi-scale biomedical imaging, *Chem. Soc. Rev.* 51 (2022) 9445–9468.
- [20] Y. Chen, M. Wang, K. Zheng, Y. Ren, H. Xu, Z. Yu, F. Zhou, C. Liu, J. Qu, J. Song, Antimony nanopolyhedrons with tunable localized surface plasmon resonances for highly effective photoacoustic-imaging-guided synergistic photothermal/immunotherapy, *Adv. Mater.* 33 (2021) 2100039.
- [21] Z. Xu, M. Quintanilla, F. Vetrone, A.O. Govorov, M. Chaker, D. Ma, Harvesting Lost Photons: Plasmon and Upconversion Enhanced Broadband Photocatalytic Activity in Core@Shell Microspheres Based on Lanthanide-Doped NaYF₄, TiO₂, and Au, *Adv. Funct. Mater.* 25 (2015) 2950–2960.
- [22] A.I. Kuznetsov, A.E. Miroshnichenko, M.L. Brongersma, Y.S. Kivshar, B. Luk'yanchuk, Optically resonant dielectric nanostructures, *Science* 354 (2016) aag2472.
- [23] J. Zhao, S. Xue, R. Ji, B. Li, J. Li, Localized surface plasmon resonance for enhanced electrocatalysis, *Chem. Soc. Rev.* 50 (2021) 12070–12097.
- [24] W. Yang, C. Bu, M. Zhao, Y. Li, S. Cui, J. Yang, H. Lian, Full-spectrum utilization of ZIF-67/Ag NPs/NaYF₄:Yb,Er photocatalysts for efficient degradation of sulfadiazine: upconversion mechanism and DFT calculation, *Small* 20 (2024) 2309972.
- [25] C. Lu, X. Cai, X. Liu, D. Tian, B. Li, J. Li, Z. Lou, Constructing plasmonic electron acceptors on TiO₂ for full-spectrum-driven photocatalytic hydrogen generation, *J. Mater. Chem. A* 12 (2024) 5909–5917.
- [26] C. Jia, X. Kan, X. Zhang, G. Lin, W. Liu, Z. Wang, S. Zhu, D. Ju, J. Liu, Construction of frustrated Lewis pairs on TiO₂-x derived from perovskite for enhanced photocatalytic CO₂ reduction, *Chem. Eng. J.* 427 (2022) 131554.
- [27] L. Marciniak, W. Piotrowski, M. Szymczak, C.D.S. Brites, V. Kinzhybalov, H. Suo, L. D. Carlos, F. Wang, The butterfly effect: multifaceted consequences of sensitizer concentration change in phase transition-based luminescent thermometer of LiYO₂:Er³⁺,Yb³⁺, *ACS Appl. Mater. Interfaces* 16 (2024) 26439–26449.
- [28] C. Wang, L. Xu, H. Jin, C. Li, Z. Zhang, L. Li, Y. Chen, J. Su, N. Liu, J. Lai, F. Long, X. Jiang, Y. Gao, Yb/Er coordinatively doping in bilayer WSe₂ for fascinating up-conversion luminescence, *Nano Energy* 78 (2020) 105317.
- [29] Z. An, Q. Li, J. Huang, L. Tao, B. Zhou, Selectively manipulating interactions between lanthanide sublattices in nanostructure toward orthogonal upconversion, *Nano Lett.* 23 (2023) 6241–6248.
- [30] J. Huang, L. Yan, Z. An, H. Wei, C. Wang, Q. Zhang, B. Zhou, Cross relaxation enables spatiotemporal color-switchable upconversion in a single sandwich nanoparticle for information security, *Adv. Mater.* 36 (2024) 2310524.
- [31] B. Lei, L. Lu, H. Sun, Modulation of phosphor luminescence performance by high concentration self-sensitization of Er and Ho–Yb ion co-doping under 1550 nm excitation, *J. Mater. Chem. C* 12 (2024) 9784–9794.
- [32] N. Chundi, E. Ramasamy, S. Koppoju, S. Mallick, A. Kottantharayil, S. Sakthivel, Quantum-sized TiO₂ particles as highly stable super-hydrophilic and self-cleaning antisoiling coating for photovoltaic application, *Sol. Energy* 258 (2023) 194–202.
- [33] J. Wang, S. Zheng, H. Zhang, Y. Wu, J. Zhang, J. Liu, X. Zhu, Y. Zhang, Unraveling the growth process of core-shell structured upconversion nanoparticles: implications for color tuning of upconversion luminescence, *ACS Appl. Nano Mater.* 6 (2023) 6398–6406.
- [34] X. Liu, Z. Chen, H. Zhang, Y. Fan, F. Zhang, Independent luminescent lifetime and intensity tuning of upconversion nanoparticles by gradient doping for multiplexed encoding, *Angew. Chem. Int. Ed.* 60 (2021) 7041–7045.
- [35] C. Hu, J. Yin, S. Xun, L. Zhu, H. Li, M. He, P. Wu, H. Li, W. Zhu, Constructing interface chemical coupling S-scheme heterojunction MoO₃-x@PPy for enhancing photocatalytic oxidative desulfurization performance: adjusting LSPR effect via oxygen vacancy engineering, *Appl. Catal., B: Environment and Energy* 355 (2024) 124155.
- [36] S.-M. Lee, P. Dhar, H. Chen, A. Montenegro, L. Liaw, D. Kang, B. Gai, A. V. Benderskii, J. Yoon, Synergistically enhanced performance of ultrathin nanostructured silicon solar cells embedded in plasmonically assisted, multispectral luminescent waveguides, *ACS Nano* 11 (2017) 4077–4085.
- [37] J. Jia, J. Dong, J. Lin, Z. Lan, L. Fan, J. Wu, Improved photovoltaic performance of perovskite solar cells by utilizing down-conversion NaYF₄:Eu³⁺ nanophosphors, *J. Mater. Chem. C* 7 (2019) 937–942.
- [38] S. Gu, Z. Lu, S. Zou, C. Wu, C. Peng, M. Ni, Z. Chen, H. Huang, H. Sun, H. Wang, X. Zhang, X. Su, In situ generating YVO₄:Eu³⁺, Bi³⁺ downshifting phosphors in SiO₂ antireflection coating for efficiency enhancement and ultraviolet stability of silicon solar cells, *Sol. RRL* 7 (2023) 2300215.
- [39] M. Schoenauer Sebagn, Z. Hu, K. de Oliveira Lima, H. Xiang, P. Gredin, M. Mortier, L. Billot, L. Aigouy, Z. Chen, Microscopic evidence of upconversion-induced near-infrared light harvest in hybrid perovskite solar cells, *ACS Appl. Energy Mater.* 1 (2018) 3537–3543.
- [40] Z. Zhang, J. Ju, X. Qin, H. Yan, M. Shen, C. Chen, F. Na, Enhancing conversion efficiency of crystalline silicon photovoltaic modules through luminescent down-shifting by using Eu³⁺–Zn²⁺-complexes, *Mater. Chem. Phys.* 290 (2022) 126599.
- [41] L. Wang, H. Chen, W. Wang, F. Hsu, H. Huang, R. Kuo, W. Li, H. Tian, C. Yeh, Boosting upconversion efficiency in optically inert shelled structures with electroactive membrane through electron donation, *Adv. Mater.* 36 (2024) 2404120.
- [42] H. Zhang, H. Wei, L. Xu, Y. Li, Z. Song, D. Zhou, Q. Wang, Z. Long, Y. Yang, Y. Wen, J. Han, Y. Gao, J. Qiu, Chiral inorganic nanostructured BiOCl co-doped with Er³⁺/Yb³⁺ exhibits circularly polarized luminescence and enhanced upconversion luminescence, *Ceram. Int.* 49 (2023) 30436–30442.
- [43] M. Lederer, H. Rijckaert, A.M. Kaczmarek, Understanding and hindering ion migration in Er,Yb:LiLuF₄ core-shell nanoparticles for nanothermometers with enhanced photoluminescence, *ACS Appl. Nano Mater.* 6 (2023) 2438–2449.